

Development of magnetic graphene oxide adsorbent for the removal and preconcentration of As(III) and As(V) species from environmental water samples

Hamid Rashidi Nodeh¹ · Wan Aini Wan Ibrahim^{1,2}  · Imran Ali³ · Mohd Marsin Sanagi^{1,4}

Received: 25 October 2015 / Accepted: 19 January 2016 / Published online: 6 February 2016
© Springer-Verlag Berlin Heidelberg 2016

Abstract New-generation adsorbent, $\text{Fe}_3\text{O}_4@\text{SiO}_2/\text{GO}$, was developed by modification of graphene oxide (GO) with silica-coated (SiO_2) magnetic nanoparticles (Fe_3O_4). The synthesized adsorbent was characterized using Fourier transform infrared spectroscopy, X-ray diffractometry, energy-dispersive X-ray spectroscopy, and field emission scanning electron microscopy. The developed adsorbent was used for the removal and simultaneous preconcentration of As(III) and As(V) from environmental waters prior to ICP-MS analysis. $\text{Fe}_3\text{O}_4@\text{SiO}_2/\text{GO}$ provided high adsorption capacities, i.e., 7.51 and 11.46 mg g^{-1} for As(III) and As(V), respectively, at pH 4.0. Adsorption isotherm, kinetic, and thermodynamic were investigated for As(III) and As(V) adsorption. Preconcentration of As(III) and As(V) were studied using magnetic solid-phase extraction (MSPE) method at pH 9.0 as the adsorbent showed selective adsorption for As(III) only in pH range 7–10. MSPE using $\text{Fe}_3\text{O}_4@\text{SiO}_2/\text{GO}$ was developed with good linearities (0.05–2.0 ng mL^{-1}) and high coefficient of determination ($R^2=0.9992$ and 0.9985) for As(III)

and As(V), respectively. The limits of detection (LODs) ($3\times\text{SD}/m$, $n=3$) obtained were 7.9 pg mL^{-1} for As(III) and 28.0 pg mL^{-1} for As(V). The LOD obtained is 357–1265 \times lower than the WHO maximum permissible limit of 10.0 ng mL^{-1} . The developed MSPE method showed good relative recoveries (72.55–109.71 %) and good RSDs (0.1–4.3 %, $n=3$) for spring water, lake, river, and tap water samples. The new-generation adsorbent can be used for the removal and simultaneous preconcentration of As(III) and As(V) from water samples successfully. The adsorbent removal for As(III) is better than As(V).

Keywords Magnetic nanoparticles · Magnetic graphene oxide · As(III) and As(V) removal · Magnetic solid-phase extraction · Adsorption isotherm · Kinetic · Thermodynamic

Introduction

Approximately 150 million people are involved with arsenic contamination in drinking water. The most affected countries are the USA, China, Chile, Bangladesh, Taiwan, Mexico, Argentina, Poland, Canada, Hungary, Japan, and India (Jain and Ali 2000). Bangladesh is extremely overshadowed with arsenic contamination, i.e., 900 villages have groundwater contaminated with arsenic more than the maximum allowance limit. In Bangladesh, skin lesions caused by arsenic was observed first time in 1987, but international attention to crisis came in 1995 (Ali 2012). Arsenic comes as natural occurrence and discharged of by-product of petroleum, chemical waste, glass, and ceramic manufacturing into water sources (Pan et al. 2010). Removal of arsenic from water is a significant problem because in natural water, arsenic is found as arsenite (As(III)), i.e., H_3AsO_3 , H_2AsO_3^- , HAsO_3^{2-} , and arsenate (As(V)) (i.e., H_3AsO_4 , H_2AsO_4^- , HAsO_4^{2-} , and AsO_4^{3-}) (Ali et al. 2011; Beker et al.

Responsible editor: Santiago V. Luis

✉ Wan Aini Wan Ibrahim
wanaini@kimia.fs.utm.my

¹ Department of Chemistry, Faculty of Science, Universiti Teknologi Malaysia, 81310 UTM, Johor Bahru, Johor, Malaysia

² Separation Science and Technology Group, Frontier Materials Research Alliance, Universiti Teknologi Malaysia, 81310 UTM, Johor Bahru, Johor, Malaysia

³ Department of Chemistry, Jamia Millia Islamia (Central University), New Delhi 110025, India

⁴ Ibnu Sina Institute for Scientific and Industrial Research, Universiti Teknologi Malaysia, 81310 UTM, Johor Bahru, Johor, Malaysia

2010). It is well known that the toxicity of arsenite is 60 times more than arsenate (Ali et al. 2014). According to the drinking water guidelines, World Health Organization (WHO) has reduced the concentration of arsenic in drinking water from 50.0 to 10.0 ng mL⁻¹ (WHO 2006). Removal and simultaneous preconcentration of arsenic species have been reported using electrocoagulation atomic fluorescence spectrophotometry (Song et al. 2014), hydride generation atomic fluorescence spectrometry (Chen and Tuanwei 2014), high-performance liquid chromatography-mass spectrometry (Morado Piñeiro et al. 2013), hydride generation prior to inductively coupled plasma mass spectrometry (ICP-MS) (Musil et al. 2014), and pH treatment prior to ICP-MS analysis (Huang et al. 2011; Shipley et al. 2009). The method based on pH is simple and convenient since it is easy, fast, and highly sensitive toward arsenic ions. Preconcentration of inorganic arsenic species using solid-phase extraction (SPE) method was reported successfully (Fang et al. 2013). SPE prior to ICP-MS has been reported separately by Huang et al. (2011), Chen et al. (2009a), and Chen et al. (2009b). Adsorption process is simple, easy to handle, no need for reagent addition, low cost, and has stable operation (Habuda-Stanić and Nujčić 2015).

Graphene oxide (GO) is a single-sheet, two-dimensional nanostructure and rich in delocalize π - π electron system with high surface area (Dreyer et al. 2014; Sanghavi et al. 2015; Xiu et al. 2015). The presence of various oxygen functional groups (carboxyl, hydroxyl, and epoxy groups) on GO are responsible for strong van der Waal's interactions and hydrogen bonding which are responsible for high sorption of metal ions. Thus, GO provides electrostatic interactions and van der Waal's forces, which are ideal for SPE sorbent (Sitko et al. 2013). GO has impressive adsorption capacity toward metal ions such as Ag(I), Fe(II), Fe(III), Cu(II), Pb(II), Co(II), Cr(II), Bi(III), Ni(I), and Mn(II) ions (Laure et al. 2013; Wang et al. 2012a) and also arsenic removal (Kumar et al. 2014; Wang et al. 2014). The positive charges of GO in acidic media showed high electrostatic interactions toward inorganic arsenic species (Chandra et al. 2010; Luo et al. 2012, 2013), leading to adsorption of 1.0 ng mL⁻¹ arsenic on GO-based composite (~99.99 % adsorption) (Chandra et al. 2010) which is higher than honeycomb briquette cinders (97.0 %) (Sun et al. 2014). Adsorption on GO is quite reliable but tedious, time-consuming, and involving high volume of water samples. To overcome these problems, magnetic nanoparticles (MNPs) were dispersed on GO sheets and extracted very quickly by an external magnetic field, without the need for filtration, centrifugation, and vacuum pump (Azam and Mohammad 2015; Wan Ibrahim et al. 2015; Yadollah et al. 2015).

Silica nanoparticles protect the MNPs in acidic medium and also increase the active sites for functionalization. The Fe₃O₄@SiO₂/GO showed high adsorption capacity (2–100-fold) for As(III) and As(V) as compared to unmodified Fe₃O₄ NPs and carbon nanofiber (CNF) (Chen et al. 2009b).

The newly developed Fe₃O₄@SiO₂/GO adsorbent was successfully used in MSPE method for the simultaneous preconcentration of the two inorganic arsenic species. The potential of the adsorbent in the removal of As(III) and As(V) was also assessed. The proposed MSPE provided excellent analytical performances, i.e., low limit of detection (LOD), high enrichment factor, good repeatability, and reproducibility. The adsorbent was more efficient in the removal of As(III) compared to As(V). The results of these findings are discussed herein.

Experimental

Materials

Sulfuric acid (98 %), nitric acid (65 %), hydrochloric acid (37 %), and ethanol (97 %) were obtained from QReC (Selangor, Malaysia). Hydrogen peroxide, potassium permanganate, L-cysteine and ammonia solution (32 %), iron(III) chloride hexahydrate (FeCl₃·6H₂O), ammonium iron(II) sulfate hexahydrate ((NH₄)₂Fe(SO₄)₂·6H₂O), arsenic trioxide, and arsenic pentoxide were obtained from Merck (Schuchardt, Germany). Graphite powder and tetraethoxysilane (TEOS) were obtained from Sigma-Aldrich (St. Louis, MO, USA). Four environmental water samples analysed in this study were of spring, river, lake, and tap water. Spring water was collected from Gunung Pulai (40 km distance from UTM). Lake water was collected from UTM, Skudai, Johor (50 cm below earth surface). The river water was collected in UTM near Centre of Information and Communication Centre and tap water was from the Department of Chemistry Laboratory, UTM.

Instrumentation

FTIR spectrum was recorded in the range of 400–4000 cm⁻¹ using a 1600 series Perkin Elmer Spectrum FTIR (MA, USA). Orbital shaker from Chung Shin RD (Taiwan, ROC) was used for samples agitation. An ICP-MS ELAN6100 spectrometer from Perkin Elmer (MA, USA) was used for the determination of As(III) and As(V). A D8-Advance X-ray diffractometer (XRD) from Bruker (Karlsruhe, Germany) was used for particle analysis with Cu K α radiation (λ =1.54060 Å), high quality mode, voltage 40 kV and current 40 mA. A Zeiss Supra 35VP scanning electron microscope from Carl Zeiss, Inc., (MN, USA) was used for the morphology and elemental analysis of the synthesized adsorbent.

ICP-MS conditions and calibration

An ICP-MS system was used for As(III) and As(V) detection. The stock solutions of As(III) and As(V) were prepared using As₂O₃ and As₃O₅, respectively. An amount of 0.0132 g

As₂O₃ and 0.0135 g As₃O₅ were separately weighed and transferred to two separate 10-mL volumetric flasks. These compounds were first dissolved in NaOH solution (0.4 g in 2.0 mL) as arsenic salts are fully dissolved in NaOH and 0.2 mL HCl (37 %) was added to neutralize the pH of the sample solution. Then, deionized water was added until mark to give a solution concentration of 1000 mg L⁻¹. Diluted standard solutions were used in further analysis, i.e., calibration, removal, and MSPE procedure. The ICP instrument was calibrated with different concentrations of As(III) and As(V) solutions. An excellent coefficient of determination (*R*²) was obtained (0.9999) for both As(III) and As(V) in the range of 1.0 to 50.0 ng mL⁻¹ (% RSD 0.01–0.2, *n* = 3). The instrument LOD (LOD = 3 × SD_{blank} / *m*) was calculated as 0.127 ng mL⁻¹. Thus, only in removal process dilution factor was used due to high residual concentration of arsenic species. Polyatomic and isobar interferences are a concern in ICP-MS system. ArCl⁺ may interfere with arsenic measurements as it exists at *m/z* 75. Thus, for the reduction of interferences, a correction factor (Eq. 1) was investigated based on blank signal. The correction factor was calculated using Eq. (1).

$${}^{75}\text{As} = \left(\text{signal}_{(75\text{As})} - 3.132 \times \text{signal}_{(75\text{ArCl})} \right) \quad (1)$$

Synthesis of magnetic nanocomposites

Synthesis of graphene oxide

GO was synthesized from graphite using a simple oxidation method. The natural graphite was powdered, and about 2.0 g was dispersed in a mixture of 20 mL HNO₃ (65 %) and 30 mL H₂SO₄ (97 %) for 24 h. Then, KMnO₄ (3.0 g) was added slowly to the mixture with continuous magnetic stirring at 50 °C for 20 h. The mixture was poured into ice (300 g) followed with the addition of 3.0 mL H₂O₂ (30 %) to produce a totally yellow product. The yellow product was diluted with deionized water (800 mL) and left overnight at room temperature until precipitate form. The supernatant was decanted, and the precipitate was washed using water until a neutral pH was obtained.

Synthesis of Fe₃O₄ magnetic nanoparticles

Fe₃O₄ MNPs were prepared by using 1.7 g of (NH₄)₂Fe(SO₄)₂ · H₂O and 3.4 g of FeCl₃ · H₂O and mixed in 20 mL of deionized water followed by sonication and degasification for 15 min. The mixture was heated at 50 °C with vigorous stirring, followed by dropwise addition of 5.0 mL of ammonia solution (32 % *v/v*) until black precipitate was formed. The heat was turned off, and the mixture was continuously and vigorously stirred for 3 h. The product obtained was then washed four times with

excess deionized water (200 mL) and oven dried at 80 °C for 24 h.

Preparation of Fe₃O₄@SiO₂

The most popular sol–gel synthesis method was used for coating Fe₃O₄ using silica, SiO₂. Briefly, 500 mg of the synthesized Fe₃O₄ MNPs was dispersed in 100 mL of water/ethanol mixture (1:1, *v/v*), followed by the addition of 5.0 mL of ammonia solution (32 % *v/v*) and finally 0.5 mL of tetraethoxysilane (TEOS). The mixture was shaken for 30 min and then left at room temperature for 24 h. The solid obtained was washed with 100 mL of a mixture of deionized water/ethanol (1:1, *v/v*) and dried to produce slightly dark brown Fe₃O₄@SiO₂.

Preparation of Fe₃O₄@SiO₂/GO

The new adsorbent (Fe₃O₄@SiO₂/GO) was synthesized using the following simple procedure. About 50.0 mL of the synthesized GO (yellow solution, ~100 mg) was transferred to a beaker, and the pH was adjusted to ~10 using NaOH (1 M) and sonicated for 30 min. Next, 10 mg of the synthesized Fe₃O₄@SiO₂ was dispersed into the GO yellow solution with vigorous stirring for 5 h at room temperature. Then, the supernatant was decanted after the black precipitate was separated from solution using an external magnet. The black precipitate was washed two times with deionized water (300 mL) and dried at 80 °C for 24 h. Finally, the dark black powder (Fe₃O₄@SiO₂/GO) was obtained as a new product. Figure 1 shows the schematic synthesis route for the preparation of magnetic adsorbent Fe₃O₄@SiO₂/GO.

Adsorption of arsenic species

The adsorption of As(III) and As(V) in water samples on the synthesized Fe₃O₄@SiO₂/GO nanocomposite was performed in batch adsorption process. Magnetic adsorbent (50 mg) was added into 50 mL of As(III) and As(V) solution with different concentration (0.1–20 mg L⁻¹) under shaking for 60 min (250 rpm) at pH 4. Then, the adsorbent was separated from solution with the assistance of an external magnet. The effect of pH on adsorption was carried out over a pH range of 3–11 using 50 mL water sample containing 1.0 mg L⁻¹ concentration of each of As(III) and As(V). The solution was shaken for 60 min (250 rpm). The solution pH was adjusted using HCl (0.1 M) and NaOH (0.1 M).

The effect of adsorbent dosage on the adsorption of As(III) and As(V) were investigated by addition of different amounts of the magnetic adsorbents (10–80 mg) into 50-mL solutions of 1.0 mg L⁻¹ of each As(III) and As(V) at pH 4.

The effect of adsorption time on As(III) and As(V) adsorption was studied in the range of 5–120 min using 40.0 mg of the adsorbent. The effect of temperature on the adsorption of

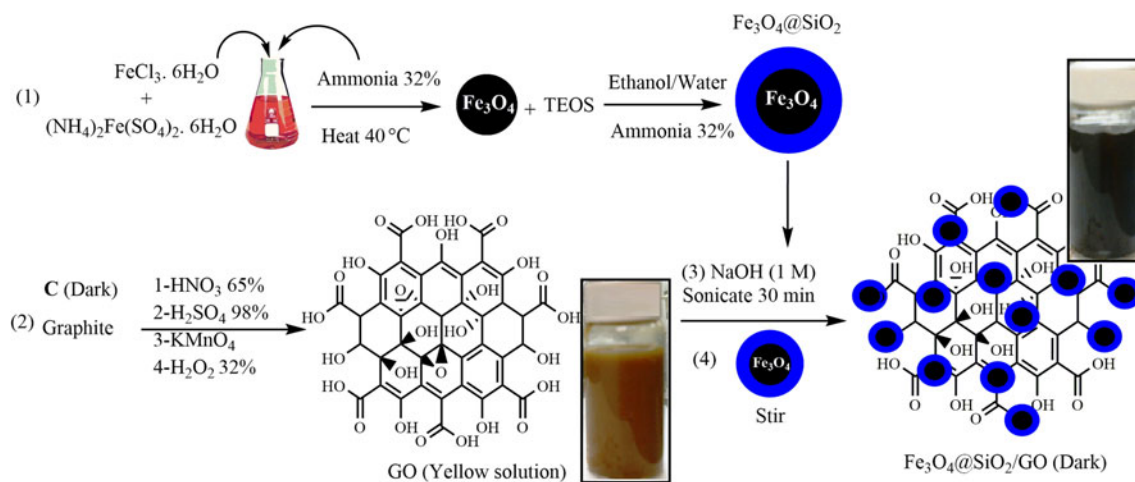


Fig. 1 Schematic synthesis route for the preparation of $\text{Fe}_3\text{O}_4@/\text{SiO}_2/\text{GO}$ nanocomposite using sol-gel and solvothermal process

As(III) and As(V) on the $\text{Fe}_3\text{O}_4@/\text{SiO}_2/\text{GO}$ was studied in the range from 298 to 328 K for 30 min (250 rpm) at pH 4. Water samples (50 mL) were spiked with 1 mg L^{-1} of each As(III) and As(V).

The residual concentration of As(III) and As(V) in the aqueous solution was measured using an ICP-MS system. The equilibrium adsorption capacity of the magnetic adsorbent was calculated using Eq. (2) (Li et al. 2013);

$$q_e = \frac{V}{m} (C_0 - C_e) \quad (2)$$

where q_e is the equilibrium adsorption capacity (mg g^{-1}), V is the initial sample volume (L), m is the mass of adsorbent (g), and C_0 and C_e are initial and residual concentrations after equilibrium of As(III) and As(V) (mg L^{-1}), respectively. The residual concentrations were calculated using the instrument's calibration.

Preconcentration of As(III) and As(V)

Preconcentration of As(III) and As(V) was developed by using the MSPE method. As(III) and As(V) were simultaneously extracted and determined in two steps. A 70.0 mL mixture of As(III) and As(V) solution (1.0 ng mL^{-1}) was prepared followed by the addition of 40.0 mg of $\text{Fe}_3\text{O}_4@/\text{SiO}_2/\text{GO}$ adsorbent, with pH adjustment to 9.0 using NaOH (1.0 M). The solution was shaken for 30 min (250 rpm), and then, the adsorbent was collected by using an external magnet. It was then washed with 5.0 mL deionized water and desorbed using 3.0 mL HCl (1 % v/v) for 5 min. The final solution was injected into ICP-MS system to determine the As(III) species.

As(V) was calculated using the equation $[\text{As(V)} = \text{total arsenic} - \text{As(III)}]$. In order to measure the total arsenic, As(V) was reduced to As(III) using L-cysteine. Mixture (70.0 mL) of each As(III) and As(V) solution (1.0 ng mL^{-1}) was prepared and 50 mg of L-cysteine was added. It was allowed to stand for

5 min resulting in a clear solution. Then, the pH was adjusted to 9.0 and 40 mg of adsorbent was added. The solution was shaken for 30 min (250 rpm) followed by adsorbent collection using an external magnet. The adsorbent was washed with 5.0 mL deionized water, and analytes were desorbed using 3.0 mL HCl (1 % v/v) (5 min vortex assistance). The final desorbed solution was injected into ICP-MS system to determine the total arsenic concentration.

Environmental water sample preparation

Four water samples of tap, river, lake, and spring sources were collected in polyethylene bottle and covered with aluminum foil. All the water samples were analyzed in two steps, i.e., unspiked and spiked with each of the arsenic species. Unspiked process was performed for As(III) and As(V) as in previous section (preconcentration of As(III) and As(V)) without any addition of standard As(III) and As(V) solution. Spiked samples were prepared by adding 1.0 ng mL^{-1} of each As(V) and As(III) species into 70.0 mL of each of the environmental water samples. Processes and conditions were performed according to MSPE procedure in previous section. Extraction recovery percentage was calculated based on the formula $\%R = (C_{\text{final}} - C_{\text{blank}} / C_{\text{initial}}) \times 100$.

Results and discussions

Characterization of adsorbent

FTIR spectroscopy

The FTIR spectra for the prepared magnetic adsorbent are shown in Fig. 2. For $\text{Fe}_3\text{O}_4@/\text{SiO}_2$, bands at 3338 and 1640 cm^{-1} are assigned to H–O stretching and bending vibration for free or adsorbed water (Fig. 2a). Peak at 544 cm^{-1}

showed Fe–O bond from Fe₃O₄ MNPs (Wang et al. 2012b). After coating, intensity of the peak related to Fe₃O₄ decreased and extra peaks were observed at 1040 and 948 cm⁻¹ that correspond to Si–O appeared. According to the literature, the graphite spectra was approximately straight (Prabakar and Narayanan 2006) but extra sharp peaks appeared on the GO spectra (Fig. 2b). This evidence demonstrated the successful conversion of graphite to GO. Broadband at 3400 cm⁻¹ indicated O–H stretching vibration related to water and organic acid. The peak at 1714 cm⁻¹ signified C=O stretching for carboxylic groups, and C–O stretching vibration of alkoxy peak was observed at 1036 cm⁻¹. C–O stretching vibrations related to C–OH or C–O was observed at 1158 and 1120.7 cm⁻¹, respectively (Wang and Dou 2012). The band at 1620 cm⁻¹ was designated to O–H bending vibration. Aromatic C=C vibration (appeared at 1437 cm⁻¹ on the surface GO) also showed at 1215, 885, and 845 cm⁻¹ identified as epoxy groups, which is assigned to symmetric stretching, asymmetric stretching, and deformation vibrations, respectively (Oh et al. 2010). Figure 2c revealed the peaks related to GO (epoxy peaks), which were fully removed, and also, Si–O intensity was decreased followed by new weak peak being observed at 1080 cm⁻¹ possibly for C–O–Si. It has been demonstrated that the Fe₃O₄@SiO₂ nanoparticles were dispersed on GO through epoxy bond, probably epoxy ring opened followed by linking with O–H group of Fe₃O₄@SiO₂. As a result, all of these evidences proved the successful synthesis of Fe₃O₄@SiO₂/GO. After the adsorption of the As(III) and As(V) onto the Fe₃O₄@SiO₂/GO (Fig. 2d, e), two peaks appeared at 1580 and 850 cm⁻¹, which signified asymmetric stretching vibration of As–O bond. These results revealed the presence of As(III) and As(V) interaction with the adsorbent.

XRD analysis

XRD is a powerful instrument for recognition of crystalline structure of synthesized materials. The XRD of Fe₃O₄, Fe₃O₄@SiO₂, and Fe₃O₄@SiO₂/GO are shown in Fig. 3. The pattern signals for magnetite (Fe₃O₄) are shown in Fig. 3a. The XRD signals for the as prepared Fe₃O₄ appeared at 2θ values of 18.32°, 30.14°, 35.51°, 43.15°, 53.44°, 57.09°, 62.68°, 74.16°, and 89.86° (Fig. 3b). The synthesized MNPs highly matched with XRD data's pattern number 01-071-6336. For Fe₃O₄@SiO₂, a broad signal was observed at 20.44° (100) (Fig. 3c) and matched the pattern number 01-070-2516. It showed SiO₂ coating and the decreased in signal intensity of Fe₃O₄ after coating (Hui et al. 2011). Furthermore, according to Fe₃O₄@SiO₂/GO data, a significant high diffraction sharp signal was marked at 2θ=25.6° (002) (Fig. 3d) which corresponds to GO skeleton (Shubhda et al. 2012; Tang et al. 2012; Zhang et al. 2015).

The diffractive peaks of Fe₃O₄ indicated that the size of Fe₃O₄ particles were quite small (Baby and Ramaprabhu 2010). The average size of Fe₃O₄ particles calculated using the Scherrer's equation (Eqs. 3 and 4) was approximately 20 nm.

$$D = \frac{K\lambda}{\beta \cos(\theta)} \tag{3}$$

$$\beta = FWHM * \left(\frac{\pi}{180}\right) \tag{4}$$

where *D*, *λ*, and *θ* are particle size (nm), wavelength (nm), and angle related to sharp peaks, respectively. FWHM is full-width data at half maximum calculated by XRD software instrument. Value of *K* constant is from 0.85 to 0.96 for different

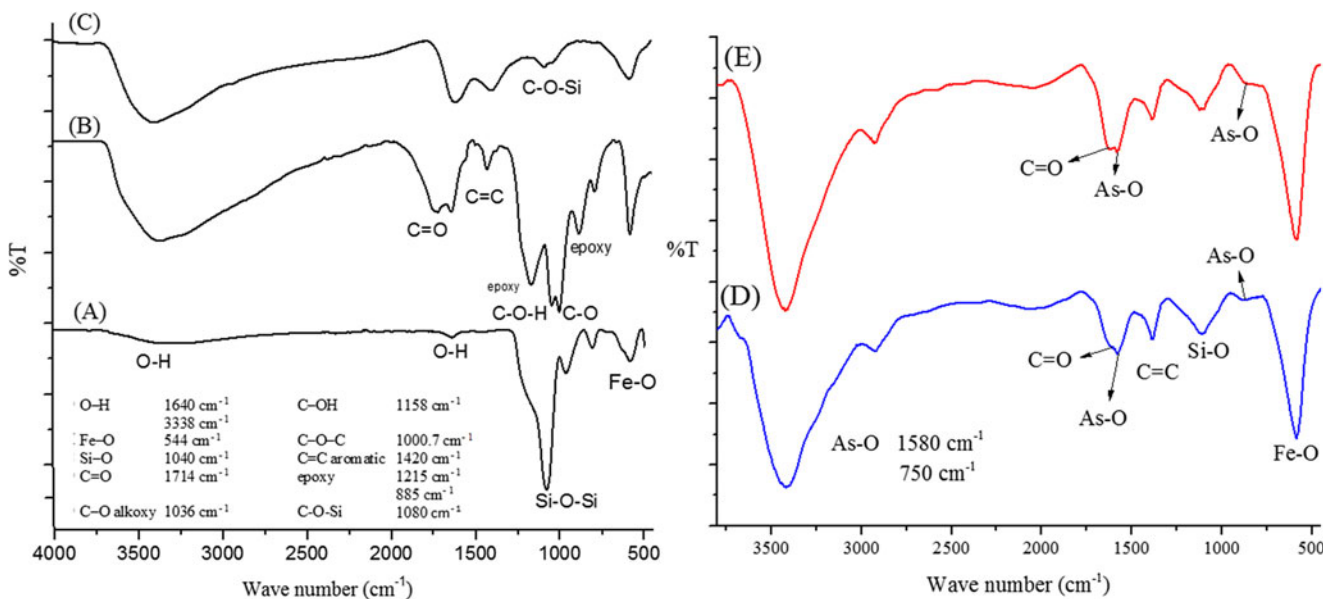
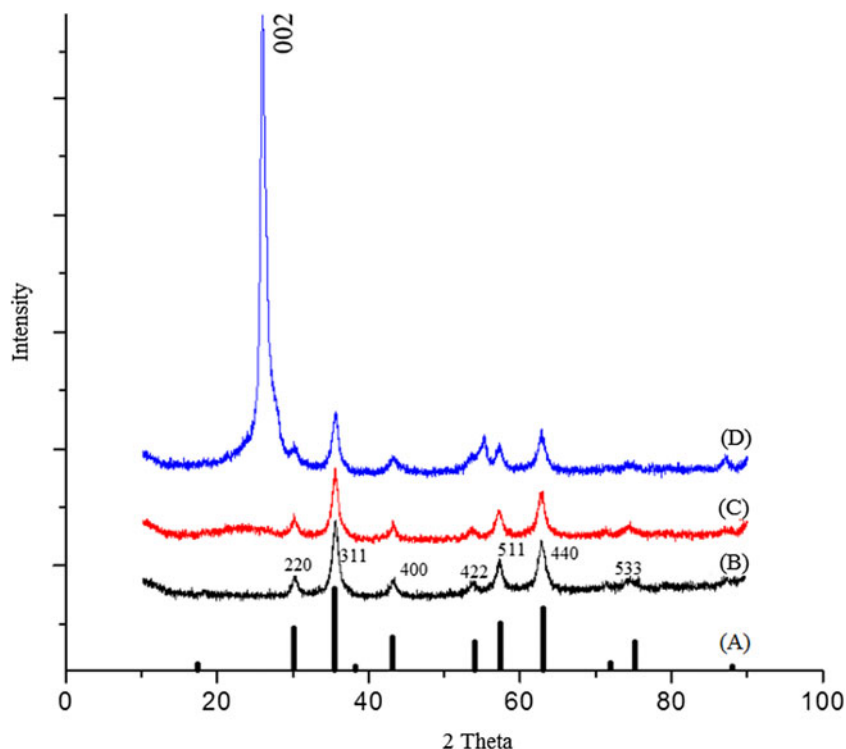


Fig. 2 FTIR spectra of **a** Fe₃O₄@SiO₂, **b** graphene oxide, **c** Fe₃O₄@SiO₂/GO (before adsorption), **d** Fe₃O₄@SiO₂/GO (after adsorption of As(III)), and **e** Fe₃O₄@SiO₂/GO (after adsorption of As(V))

Fig. 3 XRD patterns of magnetic nanocomposite: **a** Fe_3O_4 pattern, **b** synthesized Fe_3O_4 , **c** $\text{Fe}_3\text{O}_4@\text{SiO}_2$, and **d** $\text{Fe}_3\text{O}_4@\text{SiO}_2/\text{GO}$



spherical crystals. In general, K value is 0.89 for cubic Fe_3O_4 particles (Franger et al. 2004).

Micrograph analysis

The micrograph analysis of the synthesized magnetic nanocomposite based on graphene oxide was studied by using field emission scanning electron microscopy (FESEM) and transmission electron microscopy (TEM). Figure 4a, b shows the FESEM images of the adsorbent. These micrographs depicts that GO sheets with MNPs ($\text{Fe}_3\text{O}_4@\text{SiO}_2$) was functionalized appropriately on the GO sheets. The images follows the magnetic GO structure in published work (Li et al. 2015). The TEM image (Fig. 4c) also confirmed that the magnetic $\text{Fe}_3\text{O}_4@\text{SiO}_2$ nanoparticles were well dispersed on GO sheets. Figure 4d, e shows the size of $\text{Fe}_3\text{O}_4@\text{SiO}_2$ nanoparticles, where the core (Fe_3O_4) size are approximately between 7 and 15 nm and the shell (SiO_2) size is approximately 3 nm. The FESEM equipped with energy-dispersive spectrometer (EDS) was used for the elemental analysis of $\text{Fe}_3\text{O}_4@\text{SiO}_2/\text{GO}$. EDS analysis showed that the adsorbent contained 17.93 wt% iron (Fe), 5.5 wt% silicon (Si), 26.69 wt% oxygen (O), and 49.88 wt% carbon (C) (before adsorption). After adsorption process, the EDS results showed 1.73 wt% and 2.12 wt% for As(III) and As(V), respectively. These results demonstrated the arsenic species were successfully attached on the $\text{Fe}_3\text{O}_4@\text{SiO}_2/\text{GO}$.

Effect of adsorbent of mass

Adsorbent dosage of the synthesized $\text{Fe}_3\text{O}_4@\text{SiO}_2/\text{GO}$ was assessed due to the importance of adsorbent amount in adsorption efficiency removal from water samples. Five different amounts of $\text{Fe}_3\text{O}_4@\text{SiO}_2/\text{GO}$ nanocomposites were used for the adsorption of 1.0 mg L^{-1} of each As(III) and As(V) from 50.0 mL deionized water samples. The adsorption efficiency of As(III) and As(V) increased with an increase in the mass of adsorbent probably due to an increase in adsorption sites, and thus, more analytes can occupy these sites. Thus, 40.0 mg was selected as the mass of adsorbent for further analysis.

Effect of solution pH

pH plays an imperative role in separation science as it controls both degree of ionization of the materials present in the solution and the dissociation of functional group/s of the extractants (Kamboh et al. 2013). In the current study, pH of sample solution plays a crucial role in removal and simultaneous adsorption of arsenic species due to the changes of charges of arsenic species. pH of sample affects the existing forms of the analytes and their charges, as well as densities on the sorbent surface. In the pH range 3–8, As(V) exists mainly as anion H_2AsO_4^- and HAsO_4^{2-} and As(III) as uncharged H_3AsO_3 species (Huang et al. 2011). At high pH (8.0–11.5), As(V) is found as AsO_4^{3-} (Akin et al. 2012) and As(III) is found as negatively charge species, i.e., H_2AsO_3^- and HAsO_3^{2-} .

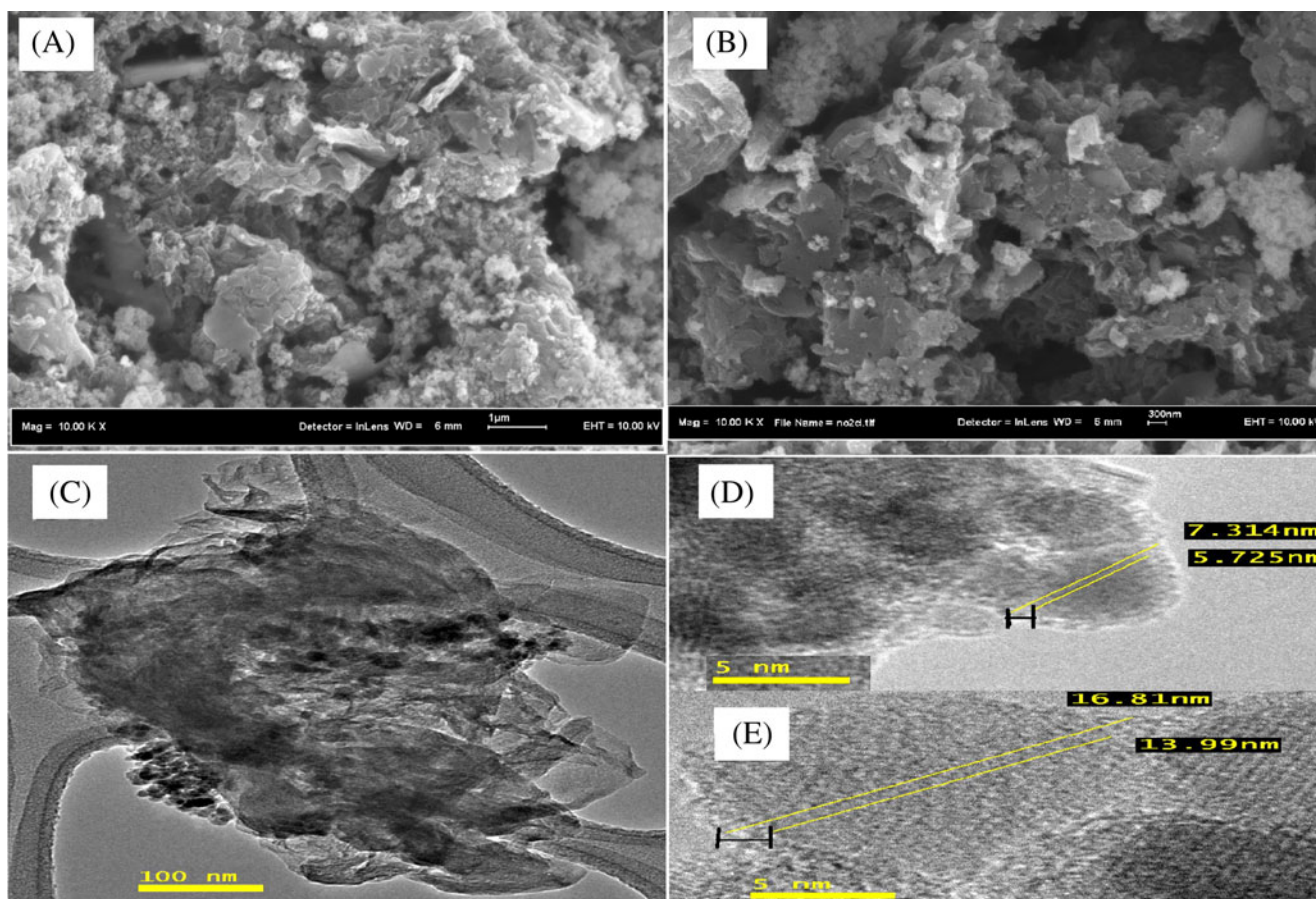


Fig. 4 FESEM micrographs of **a, b** synthesized magnetic $\text{Fe}_3\text{O}_4@\text{SiO}_2/\text{GO}$ nanocomposite and TEM micrographs of **c–e** synthesized magnetic $\text{Fe}_3\text{O}_4@\text{SiO}_2/\text{GO}$ at different magnifications

GO is independent of the ionic strength but strongly dependent on pH of the solution (Sitko et al. 2013). The pH point of zero charges (pH_{zpc}) of graphene- and GO-based material are approximately 3.9 and 6.1, respectively (Li et al. 2012; Sitko et al. 2013; Yu et al. 2013), meaning positive and negative charges on adsorbent in acidic and basic solutions, respectively.

Figure 5 shows that $\text{Fe}_3\text{O}_4@\text{SiO}_2/\text{GO}$ provides high affinity toward As(III) and As(V) adsorption at low pH as As(III) and As(V) are found as H_3AsO_3 and H_2AsO_4^- , respectively. At pH greater than 7.0 and 9.0, As(V) are found as HAsO_4^{2-} and AsO_4^{3-} , respectively, which led to a strong repulsion effect with the negative charged surface of GO-based adsorbent. Thus, a decrease in recovery to less than 20 % was observed. Furthermore, at pH 7 to 9, As(III) recovery was >85 %, probably adsorption mechanism is controlled by complexation (Chandra et al. 2010). At pH 11, As(III) recovery decreased due to the presence of H_2AsO_3^- species, which formed repulsion with the negative surface of GO-based adsorbent. Thus, pH 9.0 with removal efficiency >85 % was selected as the optimum pH for selective preconcentration of As(III) for GO-based adsorbent. Otherwise, for removal process, pH 4.0 with efficiency >90 % was selected for As(III) and As(V) adsorption.

This trend was justified by previous studies of arsenic removal using $\text{Fe}_3\text{O}_4@\text{GO}$. The removal capacities of As(V) and As(III) at pH 3.0 and 9.0 were 12.0 and 5.0 mg g^{-1} and 1.5 and 8.0 mg g^{-1} , respectively. Both As(V) and As(III) were adsorbed efficiently at pH 2–5, but at pH 8.0, the % adsorption of As(III) was three times higher than As(V) (Chandra et al. 2010). Efficient adsorption (100 %) was obtained for As(V) using GO-Fe adsorbent at pH 4.0. Lower recovery (<40 %) was observed at pH 9.0 (Zhang et al. 2010), whereas high adsorption efficiency was found for As(III) at pH 3.0 (Chen et al. 2009b).

Effect of initial concentration and adsorption isotherm

The $\text{Fe}_3\text{O}_4@\text{SiO}_2/\text{GO}$ showed high adsorption capacity toward As (III) and As(V) (Fig. 6a). At low concentration, the adsorption capacities of As(III) and As(V) were found to increase but reached to equilibrium on further increasing the concentrations.

The adsorption isotherm was studied using three different models namely Langmuir, Freundlich, and Temkin (Li et al. 2013). The values of the constants of these models are given in Table 1. In Langmuir equation, q_m is the maximum adsorption

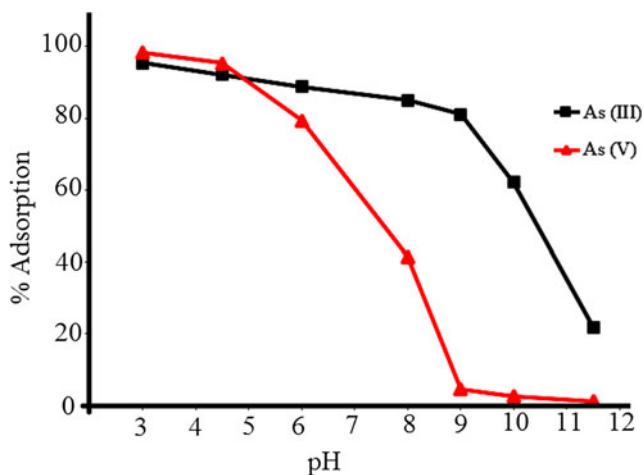


Fig. 5 Effect of solution pH on adsorption efficiencies of As(III) and As(V) extraction

capacity (mg g^{-1}). q_e is the experimental adsorption capacity that was calculated using Eq. (2), k is Langmuir constant (L mg^{-1}), and C_e is the residual concentration in the solution after extraction. The values of determination of coefficient (R^2) in Langmuir isotherm for As(III) and As(V) were 0.9989 and 0.9977, respectively, indicating the applicability of this model. The theoretical adsorption capacity was obtained by plotting C_e/q_e versus C_e (Fig. 6b). $1/q_m$ and q_m equals to the slope of line and maximum capacity, respectively (Feng et al. 2012). Value of k was calculated from the intercept. The calculated q_m value was 7.51 and 11.46 mg g^{-1} for As(III) and As(V), respectively. The values obtained were higher than the maximum capacity obtained for As(III) and As(V) using hematite@ Fe_3O_4 (Simeonidis et al. 2011) and Porous Sintered Hematite Bodies (Carabante et al. 2014). Heterogeneous surface adsorption is explained by Freundlich model (Luo et al. 2014). It shows that the adsorption mechanism is controlled by physical adsorption (i.e., van der Waal's interaction), followed by multilayer adsorption. In Freundlich equation, K_F and n are the adsorption isotherm constants, which show heterogeneous adsorption capacity $[(\text{mg/g})/(\text{mg/g})^{1/n}]$ (Ali et al. 2014). K_F and n were calculated from the intercept ($\log q_e = b$) and the slope ($1/n = m$) of plotting $\log q_e$ versus $\log C_e$. Freundlich model showed that the theoretical q_e was comparable with experimental q_e because the values of n obtained were 1 to 10. This trend showed favorable adsorption for As(III) and As(V) onto magnetic GO-based adsorbent. However, the Langmuir model fit the isotherms better, although both models described the experimental data well (Fig. 6 and Table 1). Mesoporous alumina (MA(400)) has been used for As(V) adsorption and they also found that the Langmuir equation provided a better fitting (Han et al. 2013).

Temkin isotherm shows the binding equilibrium between analytes and adsorbent. Usually high values of B provided chemisorption mechanism. In Temkin equation, A is

equilibrium constant (L/g). B is the constant related to heat of sorption (J/mol) (Luo et al. 2014). A and B can be calculated from the intercept ($\ln A = b/B$) and slope ($B = m$) of plot q_e versus $\ln C_e$. The As(III) and As(V) adsorption also was probably controlled by physical adsorption due to low values of B constant (energy). However, the three models suggests that the sorption of As(III) and As(V) onto the $\text{Fe}_3\text{O}_4@\text{SiO}_2/\text{GO}$ was probably controlled by multiple interaction mechanisms or processes (Shengsen et al. 2015).

Kinetic study

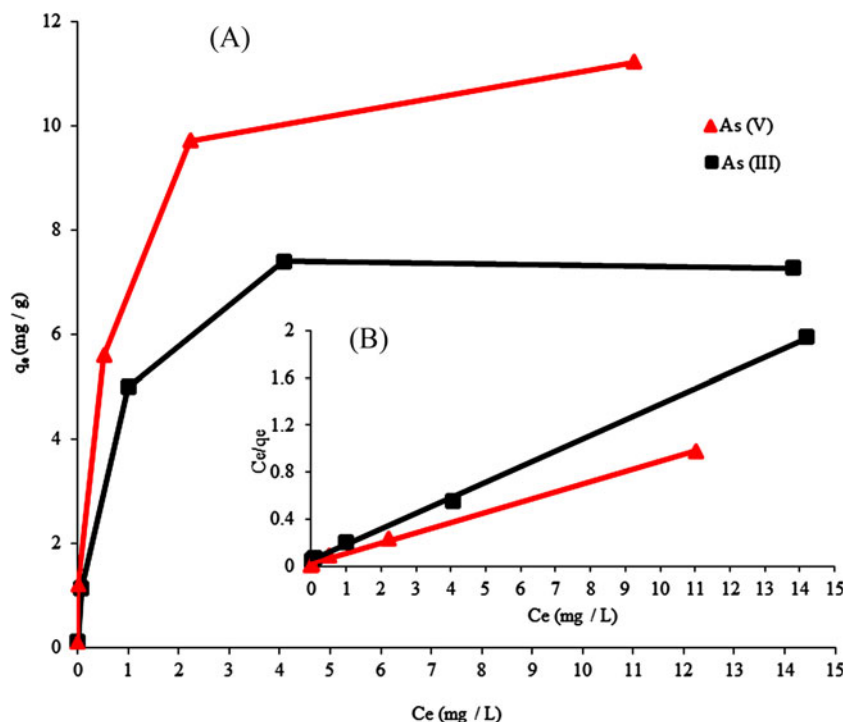
The kinetic study was carried out using contact time for the adsorption of As(III) and As(V) on the magnetic adsorbent. Figure 7a shows the increase of adsorption capacity until the contact time reached 30 min, and thereafter, it attained equilibrium.

The kinetic model was investigated using pseudo-first-order, pseudo-second-order, and intraparticle diffusion models. The equations of the three models are given in Table 2. q_e is the adsorption capacity (mg g^{-1}), and q_t is the equilibrium capacity (mg g^{-1}) at time t . k_1 and k_2 are the pseudo-first-order and pseudo-second-order adsorption rate constants (min^{-1}), respectively. k_{id} is constant for intraparticle diffusion rate. C_i is a boundary layer thickness. The values of q_e and k_1 were obtained from the linearity of pseudo-first-order rate by plotting $\ln(q_e - q_t)$ versus to t . The values of theoretical amount adsorbed and k_2 were obtained from linearity and intercept of pseudo-second-order by plotting (t/q_t) versus t (Fig. 7b). According to the data obtained (Table 2), high value of R^2 and calculated q_e (theory adsorption) from the pseudo-second-order rate indicated that the model can be applied for experimental data compared to the pseudo-first-order. The overall adsorption rates of As(III) and As(V) adsorption on the graphene-based adsorbent possibly was controlled by the sharing of electron between the analytes and adsorbent via chemisorption mechanism (Li et al. 2013). Intraparticle diffusion values (Table 2) were obtained from linearity of q_t versus $t^{1/2}$ plot. Figure 7c shows two part linearity for intraparticle diffusion model that showed As(III) and As(V) adsorption was conducted in two steps. First linearity with low slope showed slow adsorption rate. Second part with sharp slope indicated that adsorption rates of As(III) and As(V) were controlled by intraparticle diffusion (Li et al. 2013). However, this shows that the longer adsorption time can increase the adsorption of As(III) and As(V) onto the $\text{Fe}_3\text{O}_4@\text{SiO}_2/\text{GO}$ probably via chemisorption mechanism that occur between analytes and GO and also $\text{Fe}_3\text{O}_4@\text{SiO}_2$.

Thermodynamic study

The thermodynamic experiments were studied by using temperature effects on the adsorption process at three

Fig. 6 **a** Effect of initial concentrations on adsorption capacity and **b** Langmuir isotherm model linearity



different temperatures, i.e., 298, 313, and 333 K. The adsorption capacities (mg g^{-1}) were calculated using Eq. (2). The adsorption of both As(III) and As(V) increase with increase in temperature (Table 3). This trend is probably related to increase in diffusion and decrease in viscosity of the solution (Kumar et al. 2014). The increasing q_e values for both As(III) and As(V) indicated that the process was endothermic in nature (Kamboh et al. 2011). Temperature provided positive effect on adsorption since an increase in temperature increase the adsorption capacity.

Thermodynamic parameters, i.e., enthalpy changes (ΔH) and entropy changes (ΔS) were calculated according to vant Hoff’s Eq. (5). Gibb’s free energy (ΔG) was obtained from Eq. (6). These parameters explained the mechanism of adsorption process (Bhatti et al. 2013).

Thermodynamic equilibrium constant (K_c) was calculated using $K_c = q_e/C_e$ (Rashidi et al. 2010).

$$\text{Ln } K_C = \frac{-\Delta H}{RT} + \frac{\Delta S}{R} \tag{5}$$

$$-\Delta G = -RT \text{Ln } K_C \tag{6}$$

where T and R are temperature (K) and the universal gas constant ($8.3145 \text{ J mol}^{-1} \text{ K}^{-1}$), respectively. The plot of $\text{Ln } K_c$ versus $1/T(\text{K})$ gave a straight line with regression coefficient (R^2) as 0.9990 and 0.9998 for As(III) and As(V), respectively. The values of ΔH and ΔS were obtained from slope ($\Delta H = \text{slope} \times R$) and intercept ($\Delta S = \text{intercept} \times R$) of straight line. Table 3 shows values of ΔG (kJ mol^{-1}), ΔH (kJ mol^{-1}), and ΔS ($\text{J mol}^{-1} \text{ K}^{-1}$). The positive values of ΔH showed that the reaction was endothermic and positive values of ΔS

Table 1 Langmuir, Freundlich, and Temkin model constants and coefficient of determination for adsorption of As(III) and As(V) on $\text{Fe}_3\text{O}_4@\text{SiO}_2/\text{GO}$

Model	Equation	Isotherm constant	As(III)	As(V)
Langmuir	$\frac{C_e}{q_e} = \frac{C_e}{q_m} + \frac{1}{kq_m}$	q_m (mg g^{-1})	7.51	11.46
		k (L mg^{-1})	2.78	3.60
		R^2	0.9991	0.9988
Freundlich	$\text{Log } q_e = \text{Log } K_F + \left(\frac{1}{n}\right)\text{Log } C_e$	K_F [$(\text{mg/g})/(\text{mg/g})^{1/n}$]	3.04	5.74
		N	1.84	2.23
		R^2	0.9256	0.9754
Temkin	$q_e = B \text{Ln } A + B \text{Ln } C_e$	A (L g^{-1})	81.83	597.49
		B (J mol^{-1})	1.05	1.12
		R^2	0.9380	0.8928

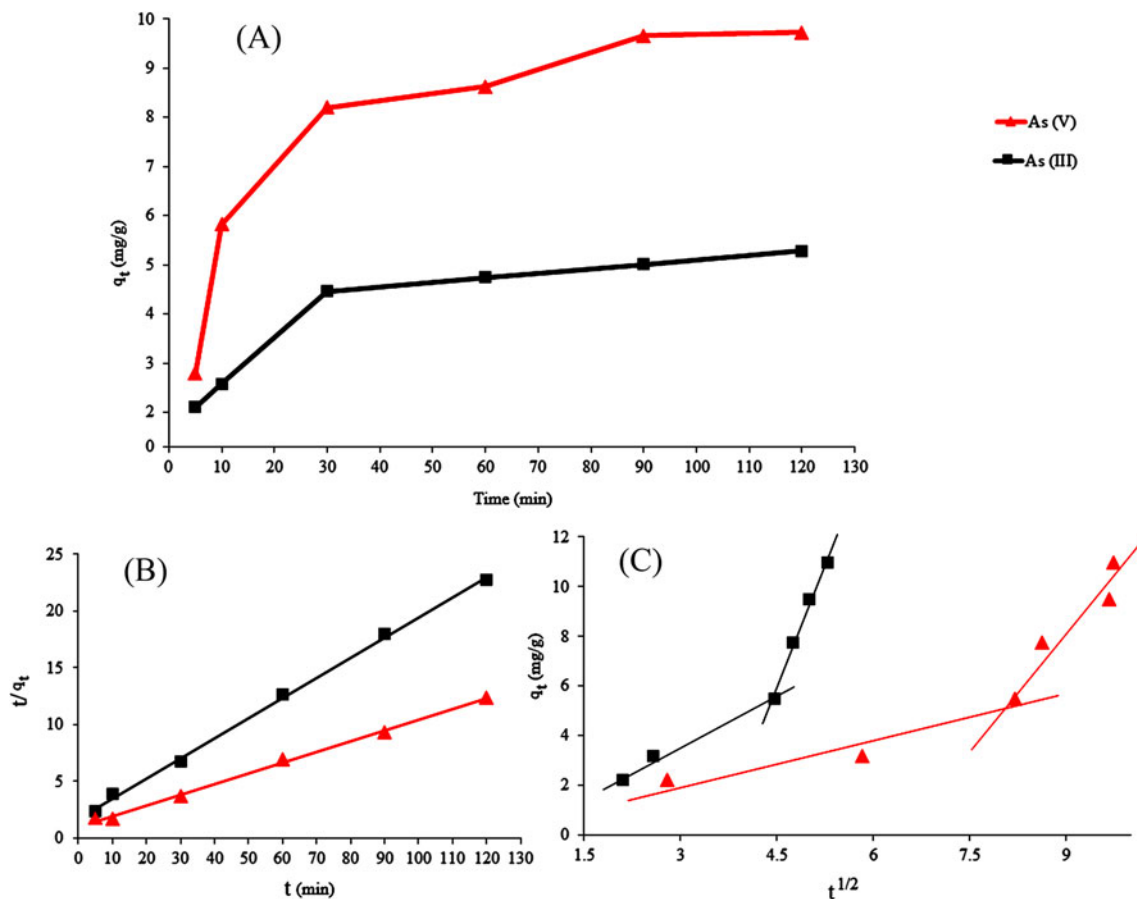


Fig. 7 Effect of **a** contact time, **b** pseudo-second-order model linearity for the adsorption of As (III) and As (V) on magnetic nanocomposite, and **c** intraparticle diffusion linearity of q_t versus $t^{1/2}$

provided randomness affinity of GO-based adsorbent toward arsenic species. Negative value of ΔG confirmed that the adsorption was spontaneous. In addition, ΔG values between 0 and -20 kJ mol^{-1} provided a physisorption process; otherwise, -80 to -400 kJ mol^{-1} indicated chemisorption process (Li et al. 2013).

Optimization of MSPE preconcentration method

The effects of different parameters on preconcentration performance of $\text{Fe}_3\text{O}_4@\text{SiO}_2/\text{GO}$ MSPE were investigated. Mass of adsorbent, solution pH, and contact time was studied in adsorption section. Effect of desorption condition was

Table 2 Kinetic modeling constants and coefficient of determination for adsorption of As(III) and As(V) on $\text{Fe}_3\text{O}_4@\text{SiO}_2/\text{GO}$

Model	Equation	Isotherm constant	As(III)	As(V)
Pseudo-first-order	$\ln(q_e - q_t) = \ln q_e - k_1 t$	q_e (mg g^{-1})	6.37	5.25
		k_1 (min^{-1})	0.0042	0.0278
		R^2	0.8181	0.9447
Pseudo-second-order	$\frac{t}{q_t} = \frac{1}{k_2 q_e^2} + \frac{1}{q_e}$	q_e (mg g^{-1})	5.64	10.66
		k_2 ($\text{g mg}^{-1} \text{min}^{-1}$)	0.022	0.015
		R^2	0.9984	0.9968
Intraparticle diffusion	$q_t = k_{id} t^{1/2} + C_i$	$K_{id,1}$	1.339	0.5866
		C_1	0.4569	0.338
		R_1^2	0.9920	0.9059
		$K_{id,2}$	6.6513	2.963
		C_2	23.991	18.415
		R_2^2	0.9925	0.9191

Table 3 Thermodynamic parameters for the adsorption of As(III) and As(V) adsorbed on Fe₃O₄@SiO₂/GO

Analyte	Temperature (K)	q _e (mg g ⁻¹)	ΔG (kJ mol ⁻¹)	ΔH (kJ mol ⁻¹)	ΔS (J mol ⁻¹ K ⁻¹)
As(III)	298	6.12	-0.45	29.27	0.09
	313	7.77	-1.87		
	328	9.23	-3.44		
As(V)	298	8.91	-2.15	40.73	0.14
	313	10.05	-4.25		
	328	11.19	-6.46		

performed using different desorption solvent, volume, and desorption time. Different acidic solution as solvents, including HCl (1 %, v/v), HNO₃ (1 %, v/v), and H₂SO₄ (1 %, v/v) were used separately in the experiment. The HCl (1 %, v/v) showed higher recoveries for the arsenic species as compared to other solvents and thus selected for further analysis. Volumes of 1 %, v/v, HCl was carried out from 0.5 to 5.0 mL. HCl desorption solvent (3.0 mL of 1 %, v/v) was enough to desorb the As(III) and As(V) from the adsorbent. Desorption time was performed for 2 min (vortex assisted). To achieve reliable recovery and intensity and high enrichment factors, sample volume plays a main role in preconcentration process (Wan Ibrahim et al. 2012). Sample volumes (10–100 mL) were considered at 1.0 ng mL⁻¹ concentration of As(III) and As(V). It was observed that 70.0 mL sample volume showed the highest recovery and was chosen as the optimum sample volume for As(III) and As(V) preconcentration.

MSPE method validation

The proposed MSPE method based on Fe₃O₄@SiO₂/GO was validated for linearity, LOD, limit of quantification (LOQ), precision (%RSD), and accuracy (% recovery). The linearity of the Fe₃O₄@SiO₂/GO MSPE technique was studied by using 70.0 mL of deionized water samples at five different concentrations of As(III) and As(V) mixture in the range of 0.05–2.0 ng mL⁻¹. The selected range studied was well below the maximum residual limit (MRL) set by WHO (10.0 ng mL⁻¹) (WHO 2006). Matrix match calibration was used for real samples. The analytical parameters (linearity, LOD, and LOQ) for Fe₃O₄@SiO₂/GO MSPE were calculated from the calibration curve. Good linearity was obtained with coefficient of determination (R²) of 0.9992 and 0.9985 was obtained for As(III) and As(V), respectively.

Table 4 shows the analytical performance of the MSPE based on Fe₃O₄@SiO₂/GO. LOD was calculated according to IUPAC definition where the limit of detection is equals to three times of standard deviation and divided by the slope of method calibration curve (LOD = 3 × SD_{blank}/m, n = 3). LODs obtained were 7.9 and 28 pg mL⁻¹ for As(III) and As(V), respectively. The LOQs obtained were 26 pg mL⁻¹ for As(III) and 79 pg mL⁻¹ for As(V) (LOQ = 3.33 × LOD, n = 3). The precision of the proposed method was assessed for repeatability (n = 3) and reproducibility (n = 9). The precision (%RSD) obtained was 0.56–4.9 % (n = 3) and 0.1–5.2 % (n = 9) for As(III) and As(V) (C = 1.0 ng mL⁻¹), respectively.

The regeneration of the synthesized adsorbent was studied for 15 adsorption-desorption cycle extractions. After each extraction process, the adsorbent was washed two times with 3.0 mL of 1 % v/v HCl and one time with 5.0 mL deionized water. The adsorbent was found to be able to be used up to 12× without showing significant lost in recovery (>80 %) and %RSD was less than 6.0 % (n = 12).

The prepared adsorbent showed lower LOD for As(III) compared to As(V). However, the LOD obtained was 1265× and 357× lower than the MRL (10 ng mL⁻¹ set by the WHO) for As(III) and As(V), respectively.

Determination of As(III) and As(V) in environmental water sample

The proposed MSPE method based on Fe₃O₄@SiO₂/GO was applied for environmental sample analyses using the optimum conditions. The experimental data from Table 5 showed high recovery >90 % (%RSD 0.1–1.4) and >72 % (%RSD 2.0–4.3) for As(III) and As(V), respectively. The low recovery of As(V) is probably related to metal ions or masking agent interferences due to anthropogenic contaminations. These

Table 4 Method calibration linearity, coefficient of determination (R²), limit of detection (LOD), limit of quantification (LOQ), and enrichment factor (EF) of As(III and As(V) using Fe₃O₄@SiO₂/GO MSPE

Species	Linearity (ng mL ⁻¹)	R ²	LOD (pg mL ⁻¹)	LOQ (pg mL ⁻¹)	EF ^a
As(III)	0.05-2	0.9994	7.9	26.1	23
As(V)	0.05-2	0.9985	28.0	92.4	23

^a Enrichment factor was calculated using EF = V_{sample} / V_{solvent}

Table 5 Analyses of real water samples for As(III) and As(V) using Fe₃O₄@SiO₂/GO MSPE

Samples	Found (ng mL ⁻¹)		% RR* (%RSD, n = 3)	
	As(III)	As(V)	As(III)	As(V)
Tap	1.59	0.97	109.71 ± 0.10	77.31 ± 3.50
River	2.07	1.33	99.73 ± 0.80	89.43 ± 3.70
Lake	2.74	1.45	90.66 ± 0.10	72.55 ± 4.30
Spring	1.76	1.09	101.88 ± 1.40	79.42 ± 2.01

*%Relative recovery was calculated as $\%RR = (C_{\text{found}} - C_{\text{real}} / C_{\text{spiked}}) \times 100$ (Rezaee et al. 2006). Determination of %RR and (%RSDs, n = 3) for different water samples (spiked at 1.0 ng mL⁻¹ of As(III) and As(V))

results demonstrated that the lake water matrices had little interference effect on MSPE adsorbent in comparison with other water sources.

Coexisting ions study

The effects of interference were carried out using coexisting ions according to recommended procedure (Shamsipur et al. 2014). Sample solution (50.0 mL, pH=9.0) containing 1.0 ng mL⁻¹ of each of the arsenic species and various concentrations (10–100 ng mL⁻¹) of interfering ions, i.e., Na⁺, K⁺, Ca²⁺, Mg²⁺, Fe²⁺, Cu²⁺, Pb²⁺, Fe³⁺, Cl⁻, NO₃⁻, Br⁻, PO₄³⁻, SO₄²⁻, and CO₃²⁻ were investigated. The results obtained provided no significant changes in recovery of the As(III) and As(V) in the presence of these various

ions. Probably positively charged ions becomes hydroxide (precipitate) in basic condition and also according to pH study possible negative charge ions form repulsion with net negative surface of adsorbent. Thus, the recoveries (>88 and >69 %) were obtained for As(III) and As(V), respectively. Lower recoveries for arsenic species have been reported in the literature example 80 % for As(V) (Aktera et al. 2005) and 67 % for As(V) from 100 µg L⁻¹ samples (Voice et al. 2011).

Comparison with other published results

The performance of MSPE Fe₃O₄@SiO₂/GO was compared with other reported adsorbents (Table 6 in terms of LOD, EF, q_m, and %R). The MSPE Fe₃O₄@SiO₂/GO method exhibited lower LOD as compared to conventional SPE based on silica and carbon nanofiber (CNF). The proposed Fe₃O₄@SiO₂/GO MSPE method in the current study showed acceptable enrichment factor. Fe₃O₄@SiO₂-AAPTS exhibited much higher EF due to capability of the developed adsorbent for extracting analytes from large volume of samples. The synthesized Fe₃O₄@SiO₂/GO MSPE adsorbent showed high adsorption capacity (2–100×) as compared to unmodified Fe₃O₄, hematite@Fe₃O₄ and CNF. The superiority of the developed adsorbent (current study) in comparison to the reported ones includes high percentage MSPE recoveries (109.7 %) for real sample with good %RSD (<1.4 %). In addition to this, desorption rate was fast (2 min vortex assisted) with good regeneration ability (12 adsorption-desorption cycles).

Table 6 Comparison of the analytical performance of the current study with some published works [analytes: total arsenic or As(III) and As(V)]

Adsorbents	Methods	Detector	pH	LOD (ng mL ⁻¹)	EF	q _m (mg g ⁻¹)	%RR	Ref.
Fe ₃ O ₄ @SiO ₂ /GO	MSPE	ICP-MS	4	0.0079	23	11.46	109.7	This study
Fe ₃ O ₄ /Mg–Al	MSPE	CL	6–7	0.002	80	12.7	106.7	Abdolmohammad-Zadeh and Talleb (2014)
TiO ₂	SPE	HG-AAS	4.0	0.02	40	–	98.0	Baig et al. (2009))
PTFE/APDC	SPE	HG-AAS	–	0.02	10	–	98.0	Anthemidis and Martavaltzoglou (2006)
Silica cartridges	SPE	ICP-MS	5.6	0.008	–	–	106.0	Yu et al. (2003)
Carbon nanofiber (CNF)	SPE	ICP-MS	3.0	0.045	33	2.00	106.0	Chen et al. (2009b)
Fe ₃ O ₄ NPs	Removal	HG-AAS	3.0	–	–	0.4	99.0	Akin et al. (2012)
Magnetic graphene oxide	Removal	ICP-ES	4.0	1	–	13.10	99.9	Chandra et al. (2010)
Graphene oxide/ferrite	Removal	ICP-OES	4.0	–	–	23.78	95.0	Zhang et al. (2010)
Polymer/Mn–Fe	Removal	Spectrophoto metric	3.5	>0.05	–	14.5	–	Jacukowicz-Sobala et al. (2013)
Fe/membrane	Removal	GF-AAS	5.0–8.0	–	–	–	96.0	Elcik et al. (2013)
Fe ₃ O ₄ -graphite oxide–MnO ₂	Removal	AFS	7.0	10	–	14.04	99.1	Luo et al. (2012)
Hematite@Fe ₃ O ₄	Removal	GF-AAS	7.0	–	–	1.00	98.0	Simeonidis et al. (2011)

Conclusion

The magnetic $\text{Fe}_3\text{O}_4@\text{SiO}_2/\text{GO}$ was successfully synthesized and used as an adsorbent for the simultaneous removal and preconcentration of As(III) and As(V) from several environmental waters. The $\text{Fe}_3\text{O}_4@\text{SiO}_2/\text{GO}$ provided high adsorption capacities for both As(III) As(V) at pH 4.0. Adsorbent showed selective adsorption for As(III) only in pH range 7–10, which is useful for speciation study. The arsenic removal process was validated using experimental adsorption capacity, adsorption rate, and temperature effects. Thus, adsorption experimental data fitted well with Langmuir isotherm model as compared to Freundlich model and Temkin due to high value of R^2 . Langmuir model confirmed monolayer adsorption for As(III) and As(V) on adsorbent with adsorption capacity of 7.51–11.46 mg g^{-1} . Kinetic models performed showed that adsorption rate was controlled by pseudo-second-order and intraparticle diffusion. Thermodynamic study showed that As(III) and As(V) adsorption on $\text{Fe}_3\text{O}_4@\text{SiO}_2/\text{GO}$ are spontaneous and endothermic process due to negative energy ($-\Delta G$) and positive enthalpy ($+\Delta H$), respectively. The new-generation adsorbent was successfully used for the simultaneous separation of arsenic species from water due to excellent adsorption efficiency ($>95\%$ at 0.05 ng mL^{-1} concentration of As(III) and As(V)). The proposed $\text{Fe}_3\text{O}_4@\text{SiO}_2/\text{GO}$ MSPE method exhibited lower LOD for As(III) (7.9 pg mL^{-1}) and As(V) (28.0 pg mL^{-1}). It is applicable to the determination of these two species in environmental water samples. The synthesized $\text{Fe}_3\text{O}_4@\text{SiO}_2/\text{GO}$ nanocomposite is a good alternative adsorbent for adsorption and preconcentration of As(III) and As(V) from water samples. The developed adsorbent is selective and reproducible in nature. Besides, fast extraction (or adsorption) and good regeneration capability (12 times) made this adsorbent economical in nature.

Acknowledgments The authors gratefully acknowledge the Ministry of Education (MOE) Malaysia for financial support through the Research Grants No. 10J43 and 04H22. H. R. Nodeh would like to thank UTM for the International Doctoral Fellowship (IDF) received.

References

- Abdolmohammad-Zadeh H, Talleb Z (2014) Speciation of As(III)/As(V) in water samples by a magnetic solid phase extraction based on $\text{Fe}_3\text{O}_4/\text{Mg}-\text{Al}$ layered double hydroxide nano-hybrid followed by chemiluminescence detection. *Talanta* 128:147–155. doi:10.1016/j.talanta.2014.04.070
- Akin I, Arslan G, Tor A, Ersoz M, Cengeloglu Y (2012) Arsenic(V) removal from underground water by magnetic nanoparticles synthesized from waste red mud. *J Hazard Mater* 235–236:62–68. doi:10.1016/j.jhazmat.2012.06.024
- Akter KF, Chen Z, Smith L, Davey D, Naidu R (2005) Speciation of arsenic in ground water samples: A comparative study of CE-UV, HG-AAS and LC-ICP-MS. *Talanta* 68:406–415. doi:10.1016/j.talanta.2005.09.011
- Ali I (2012) New generation adsorbents for water treatment. *Chem Rev* 112:5073–5091. doi:10.1021/cr300133d
- Ali I, Khan TA, Asim M (2011) Removal of arsenic from water by electrocoagulation and electrodialysis techniques. *Sep Purif Rev* 40:25–42. doi:10.1080/15422119.2011.542738
- Ali I, Al-Othman ZA, Alwarthan A, Asim M, Khan TA (2014) Removal of arsenic species from water by batch and column operations on bagasse fly ash. *Environ Sci Pollut Res* 21:3218–3229. doi:10.1007/s11356-013-2235-3
- Anthemidis AN, Martavaltzoglou EK (2006) Determination of arsenic(III) by flow injection solid phase extraction coupled with on-line hydride generation atomic absorption spectrometry using a PTFE turnings-packed micro-column. *Anal Chim Acta* 573–574: 413–418. doi:10.1016/j.aca.2005.12.055
- Azam S, Mohammad A (2015) Magnetic $\text{Fe}_3\text{O}_4@\text{C}$ nanoparticles modified with 1-(2-thiazolylazo)-2-naphthol as a novel solid-phase extraction sorbent for preconcentration of copper (II). *Microchim Acta* 182:257–264. doi:10.1007/s00604-014-1327-1
- Baby TT, Ramaprabhu S (2010) SiO_2 coated Fe_3O_4 magnetic nanoparticle dispersed multiwalled carbon nanotubes based amperometric glucose biosensor. *Talanta* 80:2016–2022. doi:10.1016/j.talanta.2009.11.010
- Baig JA, Kazi TG, Shah AQ, Arain MB, Afridi HI, Kandhro GA, Khan S (2009) Optimization of cloud point extraction and solid phase extraction methods for speciation of arsenic in natural water using multivariate technique. *Anal Chim Acta* 651:57–63. doi:10.1016/j.aca.2009.07.065
- Beker U, Cumbal L, Duranoglu D, Kucuk I, Sengupta A (2010) Preparation of Fe oxide nanoparticles for environmental applications: arsenic removal. *Environ Geochem Health* 32:291–296. doi:10.1007/s10653-010-9301-2
- Bhatti AA, Kamboh MA, Solangi IB, Memon S (2013) Synthesis of calix[6]arene based XAD-4 material for the removal of reactive blue 19 from aqueous environments. *J Appl Polym Sci* 130:776–785. doi:10.1002/app.39214
- Carabante I, Mouzon J, Kumpiene J, Gran M, Fredriksson A, Hedlund J (2014) Reutilization of porous sintered hematite bodies as effective adsorbents for arsenic(V) removal from water. *Ind Eng Chem Res* 53:12689–12696. doi:10.1021/ie500919d
- Chandra V, Park J, Chun Y, Lee JW, Hwang IC, Kim KS (2010) Water-dispersible magnetite-reduced graphene oxide composites for arsenic removal. *ACS Nano* 4:3979–3986. doi:10.1021/nn1008897
- Chen G, Tuanwei C (2014) SPE speciation of inorganic arsenic in rice followed by hydride-generation atomic fluorescence spectrometric quantification. *Talanta* 119:202–206. doi:10.1016/j.talanta.2013.11.016
- Chen D, Huang C, He M, Hu B (2009a) Separation and preconcentration of inorganic arsenic species in natural water samples with 3-(2-aminoethylamino) propyltrimethoxysilane modified ordered mesoporous silica micro-column and their determination by inductively coupled plasma optical emission spectrometry. *J Hazard Mater* 164:1146–1151. doi:10.1016/j.jhazmat.2008.09.022
- Chen S, Zhan X, Lu D, Liu C, Zhu L (2009b) Speciation analysis of inorganic arsenic in natural water by carbon nanofibers separation and inductively coupled plasma mass spectrometry determination. *Anal Chim Acta* 634:192–196. doi:10.1016/j.aca.2008.12.018
- Dreyer DR, Todd AD, Bielawski CW (2014) Harnessing the chemistry of graphene oxide. *Chem Soc Rev* 43:5288–5301. doi:10.1039/C4CS00060A
- Elcik H, Cakmakci M, Sahinkaya E, Ozkaya B (2013) Arsenic removal from drinking water using low pressure membranes. *Ind Eng Chem Res* 52:9958–9964. doi:10.1021/ie401393p

- Fang D, Ruizhi D, Kai Y, Xubiao L, Xinman T, Shenglian L, Lixia Y (2013) Determination of trace total inorganic arsenic by hydride generation atomic fluorescence spectrometry after solid phase extraction-preconcentration on aluminium hydroxide gel. *Microchim Acta* 180:509–515. doi:10.1007/s00604-013-0941-7
- Feng L, Cao M, Ma X, Zhu Y, Hu C (2012) Superparamagnetic high-surface-area Fe₃O₄ nanoparticles as adsorbents for arsenic removal. *J Hazard Mater* 217–218:439–446. doi:10.1016/j.jhazmat.2012.03.073
- Franger S, Berthet P, Berthon J (2004) Electrochemical synthesis of Fe₃O₄ nanoparticles in alkaline aqueous solutions containing complexing agents. *J Solid State Electrochem* 8:218–223. doi:10.1007/s10008-003-0469-6
- Habuda-Stanić M, Nujić M (2015) Arsenic removal by nanoparticles: a review. *Environ Sci Pollut Res* 22:8094–8123. doi:10.1007/s11356-015-4307-z
- Han C, Li H., Pu H., Yu H., Deng L., Huang S., Luo Y. (2013), Synthesis and characterization of mesoporous alumina and their performances for removing arsenic(V), *Chem. Eng. J.*, 217 :1–9. doi 10.1016/j.cej.2012.11.087
- Huang C, Xie W, Li X, Zhang J (2011) Speciation of inorganic arsenic in environmental waters using magnetic solid phase extraction and preconcentration followed by ICP-MS. *Microchim Acta* 173:165–172. doi:10.1007/s00604-010-0532-9
- Hui C, Shen C, Tian J, Bao L, Ding H, Li C, Tian Y, Shi X, Gao HJ (2011) Core-shell Fe₃O₄@SiO₂ nanoparticles synthesized with well-dispersed hydrophilic Fe₃O₄ seeds. *Nanoscale* 3:701–705. doi:10.1039/C0NR00497A
- Jacukowicz-Sobala I, Ociński D, Kociołek-Balawejder E (2013) Synthesis and evaluation of a novel hybrid polymer containing manganese and iron oxides as a sorbent for As(III) and As(V) removal. *Ind Eng Chem Res* 52:6453–6461. doi:10.1021/ie400478x
- Jain C, Ali I (2000) Arsenic: occurrence, toxicity and speciation techniques. *Water Res* 34:4304–4312. doi:10.1016/S0043-1354(00)00182-2
- Kamboh MA, Solangi IB, Sherazi STH, Memon S (2011) A highly efficient calix[4]arene based resin for the removal of azo dyes. *Desalination* 268:83–89. doi:10.1016/j.desal.2010.10.001
- Kamboh M, Akoz E, Memon S, Yilmaz M (2013) Synthesis of amino-substituted p-tert-butylcalix [4]arene for the removal of Chicago Sky Blue and Tropaeolin 000 Azo Dyes from aqueous environment. *Water Air Soil Pollut* 224:1–9. doi:10.1007/s11270-012-1424-x
- Kumar S, Nair RR, Pillai PB, Gupta SN, Iyengar MAR, Sood AK (2014) Graphene oxide–MnFe₂O₄ magnetic nanohybrids for efficient removal of lead and arsenic from water. *ACS Appl Mater Interfaces* 6:17426–17436. doi:10.1021/am504826q
- Laure IL, Tkachev SV, Buslaeva EY, Fatushina EV, Gubin SP (2013) The coordination chemistry of graphene oxide: Interactions with metal ions in water. *Russ J Coord Chem* 39:487–492. doi:10.1134/S1070328413070038
- Li J, Zhang S, Chen C, Zhao G, Yang X, Li J, Wang X (2012) Removal of Cu(II) and fulvic acid by graphene oxide nanosheets decorated with Fe₃O₄ nanoparticles. *ACS Appl Mater Interfaces* 4:4991–5000. doi:10.1021/am301358b
- Li Y, Du Q, Liu T, Sun J, Wang Y, Wu S, Wang Z, Xia Y, Xia L (2013) Methylene blue adsorption on graphene oxide/calcium alginate composites. *Carbohydr Polym* 95:501–507. doi:10.1016/j.carbpol.2013.01.094
- Li ZJ, Lin W, LY Y, Xiao CL, Lei M, Zheng LR, Jing Z, Yang JH, Zhao YL, Zhu ZT, Chai ZF, Shi WQ (2015) Efficient removal of uranium from aqueous solution by zero-valent iron nanoparticle and its graphene composite. *J Hazard Mater* 290:26–33. doi:10.1016/j.jhazmat.2015.02.028
- Luo X, Wang C, Luo S, Dong R, Tu X, Zeng G (2012) Adsorption of As (III) and As (V) from water using magnetite Fe₃O₄-reduced graphite oxide–MnO₂ nanocomposites. *Chem Eng J* 187:45–52. doi:10.1016/j.cej.2012.01.073
- Luo X, Wang C, Wang L, Deng F, Luo S, Tu X, Au C (2013) Nanocomposites of graphene oxide-hydrated zirconium oxide for simultaneous removal of As(III) and As(V) from water. *Chem Eng J* 220:98–106. doi:10.1016/j.cej.2013.01.017
- Luo S, Xu X, Zhou G, Liu C, Tang Y, Liu Y (2014) Amino siloxane oligomer-linked graphene oxide as an efficient adsorbent for removal of Pb(II) from wastewater. *J Hazard Mater* 274:145–155. doi:10.1016/j.jhazmat.2014.03.062
- Morado Piñeiro A, Moreda-Piñeiro J, Alonso-Rodríguez E, López-Mahía P, Muniategui-Lorenzo S, Prada-Rodríguez D (2013) Arsenic species determination in human scalp hair by pressurized hot water extraction and high performance liquid chromatography-inductively coupled plasma-mass spectrometry. *Talanta* 105:422–428. doi:10.1016/j.talanta.2012.10.070
- Musil S, Pétursdóttir ÁH, Raab A, Gunnlaugsdóttir H, Krupp E, Jr Feldmann (2014) Speciation without chromatography using selective hydride generation: inorganic arsenic in rice and samples of marine origin. *Anal Chem* 86:993–999. doi:10.1021/ac403438c
- Oh J, Jun HL, Ja CK, Hyouk RC, Youngkwan L, Taesung K, Nguyen DL, Jae DN (2010) Graphene oxide porous paper from amine-functionalized poly(glycidyl methacrylate)/graphene oxide core-shell microspheres. *J Mater Chem* 20:9200–9204. doi:10.1039/C0JM00107D
- Pan YF, Chiou C, Lin TF (2010) Adsorption of arsenic(V) by iron-oxide-coated diatomite (IOCD). *Environ Sci Pollut Res* 17:1401–1410. doi:10.1007/s11356-010-0325-z
- Prabakar SJR, Narayanan SS (2006) Surface modification of amine-functionalised graphite for preparation of cobalt hexacyanoferrate (CoHCF)-modified electrode: an amperometric sensor for determination of butylated hydroxyanisole (BHA). *Anal Bioanal Chem* 386:2107–2115. doi:10.1007/s00216-006-0854-y
- Rashidi F, Sarabi RS, Ghasemi Z, Seif A (2010) Kinetic, equilibrium and thermodynamic studies for the removal of lead (II) and copper (II) ions from aqueous solutions by nanocrystalline. *Superlattice Microsc* 48:577–591. doi:10.1016/j.spmi.2010.09.011
- Rezaee M, Assadi Y, Milani Hosseini M-R, Aghae E, Ahmadi F, Berjani S (2006) Determination of organic compounds in water using dispersive liquid–liquid microextraction. *J Chromatogr A* 1116:1–9. doi:10.1016/j.chroma.2006.03.007
- Sanghavi BJ, Gadhari NS, Kalambate PK, Karna SP, Srivastava AK (2015) Potentiometric stripping analysis of arsenic using a graphene paste electrode modified with a thiocrown ether and gold nanoparticles. *Microchim Acta* 182:1473–1481. doi:10.1007/s00604-015-1470-3
- Shamsipur M, Fattahi N, Assadi Y, Sadeghi M, Sharafi K (2014) Speciation of As(III) and As(V) in water samples by graphite furnace atomic absorption spectrometry after solid phase extraction combined with dispersive liquid–liquid microextraction based on the solidification of floating organic drop. *Talanta* 130:26–32. doi:10.1016/j.talanta.2014.06.049
- Shengsen W, Bin G, Andrew RZ, Yuncong L, Lena M, Willie GH, Kati WM (2015) Removal of arsenic by magnetic biochar prepared from pinewood and natural hematite. *Bioresour Technol* 175:391–395. doi:10.1016/j.biortech.2014.10.104
- Shiple HJ, Yean S, Kan AT, Tomson MB (2009) Adsorption of arsenic to magnetite nanoparticles: effect of particle concentration, pH, ionic strength, and temperature. *Environ Toxicol Chem* 28:509–515. doi:10.1897/08-155.1
- Shubhda S, Kiran J, Singh VN, Sukhvir S, Vijayan N, Nita D, Govind G, Senguttuvan TD (2012) Faster response of NO₂ sensing in graphene–WO₃ nanocomposites. *Nanotechnology* 23:205501. doi:10.1088/0957-4484/23/20/205501
- Simeonidis K, Gkinis T, Tresintsi S, Martinez-Boubeta C, Vourlias G, Tsiaoussis I, Angelakeris M (2011) Magnetic separation of

- hematite-coated Fe₃O₄ particles used as arsenic adsorbents. *Chem Eng J* 168:1008–1015. doi:10.1016/j.cej.2011.01.074
- Sitko R, Zawisza B, Malicka E (2013) Graphene as a new sorbent in analytical chemistry. *TrAC Trend Anal Chem* 51:33–43. doi:10.1016/j.trac.2013.05.011
- Song P, Yang Z, Xu H, Huang J, Yang X, Wang L (2014) Investigation of influencing factors and mechanism of antimony and arsenic removal by electrocoagulation using Fe-Al electrodes. *Ind Eng Chem Res* 53:12911–12919. doi:10.1021/ie501727a
- Sun B, Zhai H, Zhang LB, Zhang CX, Wu XS (2014) Removal of trace arsenic based on biomimetic separation. *Ind Eng Chem Res* 54:396–403. doi:10.1021/ie503033r
- Tang Y, Huang F, Zhao W, Liu Z, Wan D (2012) Synthesis of graphene-supported Li₄Ti₅O₁₂ nanosheets for high rate battery application. *J Mater Chem* 22:11257–11260. doi:10.1039/C2JM30624G
- Voice TC, Flores del Pino LV, Hazezov I, Long DT (2011) Field deployable method for arsenic speciation in water. *Phys Chem Earth* 36:436–441. doi:10.1016/j.pce.2010.03.027
- Wan Ibrahim WA, Veloo KV, Sanagi MM (2012) Novel sol–gel hybrid methyltrimethoxysilane–tetraethoxysilane as solid phase extraction sorbent for organophosphorus pesticides. *J Chromatogr A* 1229:55–62. doi:10.1016/j.chroma.2012.01.022
- Wan Ibrahim WA, Rashidi Nodeh H, Hassan YAE, Sanagi MM (2015) Magnetic solid-phase extraction based on modified ferum oxides for enrichment, preconcentration, and isolation of pesticides and selected pollutants. *Crit Rev Anal Chem* 45:270–287. doi:10.1080/10408347.2014.938148
- Wang X, Dou W (2012) Preparation of graphite oxide (GO) and the thermal stability of silicone rubber/GO nanocomposites. *Thermochim Acta* 529:25–28. doi:10.1016/j.tca.2011.11.016
- Wang Y, Gao S, Zang X, Li J, Ma J (2012a) Graphene-based solid-phase extraction combined with flame atomic absorption spectrometry for a sensitive determination of trace amounts of lead in environmental water and vegetable samples. *Anal Chim Acta* 716:112–118. doi:10.1016/j.aca.2011.12.007
- Wang Y, Wang L, Tian T, Hu X, Yang C, Xu Q (2012b) Automated solid-phase extraction hyphenated to voltammetry for the determination of quercetin using magnetic nanoparticles and sequential injection lab-on-valve approach. *Analyst* 137:2400–2405. doi:10.1039/C2AN35300H
- Wang C, Luo H, Zhang Z, Wu Y, Zhang J, Chen S (2014) Removal of As (III) and As (V) from aqueous solutions using nanoscale zero valent iron-reduced graphite oxide modified composites. *J Hazard Mater* 268:124–131. doi:10.1016/j.jhazmat.2014.01.009
- WHO (2006) Guidelines for drinking-water quality: first addendum to third edition, vol 1, Recommendations. World Health Organization, Geneva
- Xiu C, Shengnan W, Yongxin L, Gang W (2015) Sensing hydrogen peroxide using a glassy carbon electrode modified with in-situ electrodeposited platinum-gold bimetallic nanoclusters on a graphene surface. *Microchim Acta* 182:265–272. doi:10.1007/s00604-014-1321-7
- Yadollah Y, Mohammad F, Mahnaz A (2015) Magnetic silica nanomaterials for solid-phase extraction combined with dispersive liquid-liquid microextraction of ultra-trace quantities of plasticizers. *Microchim Acta* 182:1491–1499. doi:10.1007/s00604-015-1474-z
- Yu C, Cai Q, Guo ZX, Yang Z, Khoo SB (2003) Inductively coupled plasma mass spectrometry study of the retention behavior of arsenic species on various solid phase extraction cartridges and its application in arsenic speciation. *Spectrochim Acta B* 58:1335–1349. doi:10.1016/s0584-8547(03)00079-x
- Yu X, Tong S, Ge M, Wu L, Zuo J, Cao C, Song W (2013) Synthesis and characterization of multi-amino-functionalized cellulose for arsenic adsorption. *Carbohydr Polym* 92:380–387. doi:10.1016/j.carbpol.2012.09.050
- Zhang K, Dwivedi V, Chi C, Wu J (2010) Graphene oxide/ferric hydroxide composites for efficient arsenate removal from drinking water. *J Hazard Mater* 182:162–168. doi:10.1016/j.jhazmat.2010.06.010
- Zhang C, Ai L, Jiang J (2015) Graphene hybridized photoactive iron terephthalate with enhanced photocatalytic activity for the degradation of Rhodamine B under visible light. *Ind Eng Chem Res* 54:153–163. doi:10.1021/ie504111y